

pubs.acs.org/JPCL Letter

Stability of 20S Proteasome Configurations: Preopening the Axial Gate

Lucas W. Henderson, Edie M. Sharon, Amit K. S. Gautam, Adam J. Anthony, Martin F. Jarrold, David H. Russell, Andreas Matouschek, and David E. Clemmer*



Cite This: J. Phys. Chem. Lett. 2023, 14, 5014-5017



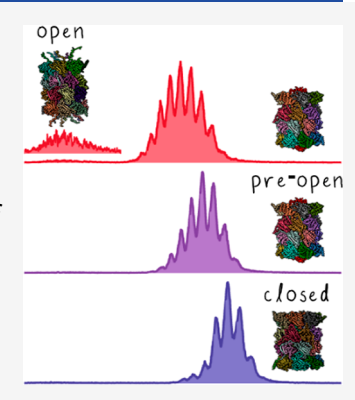
ACCESS I

III Metrics & More

Article Recommendations

Supporting Information

ABSTRACT: Mass spectrometry studies of the stability of the *S. cerevisiae* 20S proteasome from 11 to 55 °C reveal a series of related configurations and coupled transitions that appear to be associated with opening of the proteolytic core. We find no evidence for dissociation, and all transitions are reversible. A thermodynamic analysis indicates that configurations fall into three general types of structures: enthalpically stabilized, tightly closed (observed as the +54 to +58 charge states) configurations; high-entropy (+60 to +66) states that are proposed as precursors to pore opening; and larger (+70 to +79) partially and fully open pore structures. In the absence of the 19S regulatory unit, the mechanism for opening the 20S pore appears to involve a charge-priming process that loosens the closed-pore configuration. Only a small fraction (\leq 2%) of these 20S precursor configurations appear to open and thus expose the catalytic cavity.



he eukaryotic 20S proteasome from S. cerevisiae (budding yeast) is a stack of four heptameric-protein rings (Figure 1), forming a proteolytic cavity that cleaves proteins into peptides. Either, or both, of the 20S ends may bind 19S caps, generating 26S or 30S proteasomes: highly structured, ATPdriven machines that control cellular processes through regulated protein degradation.² Although mechanisms of the 26S are not entirely understood, progress characterizing intermediates and pathways involved in lid opening and threading a targeted polypeptide chain into the 20S core has been made (including high-resolution characterization of the 19S-20S interface).³ In contrast, less is known about structures and energetics of isolated 20S particles, although they can process some polypeptide chains and unstructured proteins despite lacking a 19S unit, especially during heat or oxidative stress to cells.4 Below, we examine structures and stabilities of the 20S proteasome using mass spectrometry (MS)-based techniques. Upon incubation in ammonium acetate solutions from 11 to 55 °C, we observe coexisting 20S configurations and determine ΔG , ΔH , and ΔS for these species. We interpret these results as evidence for two compact, closed-pore configurations: a tightly closed (enthalpically stabilized) form and a loosened (entropically favored) preopen configuration. Conformational changes induced upon addition of charge may be key in regulating proteolytic activity without a bound 19S cap.

Structural analysis is performed using variable-temperature electrospray ionization coupled with ion mobility spectrometry (IMS)–MS instrumentation (see SI). The 1.0 μ M 20S solutions were incubated for ~2 to 10 min at a specified

temperature (from 11 to 55 \pm 1 °C) in a capillary emitter. As electrospray droplets shrink, they undergo an evaporative cooling process, trapping ensembles of 20S species at each incubation temperature (see SI).5,6 Figure 1 shows mass spectra recorded at solution temperatures of 23, 33, and 54 °C; the peaks correspond to species having different amounts of excess positive charge, the largest of each distribution corresponding to the +58, +60, and +62 charge states, respectively (see SI for additional temperatures). Incremental changes in solution temperature cause gradual shifts in the charge state distribution (from +54 to +58 at 15 °C, to +60 to +66 at 54 °C). It is instructive to plot the weighted average of 20S charge states for each temperature (Figure 1, top right). In this analysis, a well-behaved, cooperative two-state transition would yield a sigmoidal curve having a "melting temperature" inferred from the inflection point. 5,7 The data in Figure 1 show a gradual, linear increase of ~1 charge per 6 °C, indicating that changes in the 20S charge do not follow a cooperative, twostate model.

We thus consider relative abundances of the individual charge states, also shown in Figure 1. Each displays a unique abundance profile; the maximum abundance for each state is similar, \sim 20 to 30% of the total. Disregarding low abundance

 Received:
 April 17, 2023

 Accepted:
 May 22, 2023

 Published:
 May 24, 2023





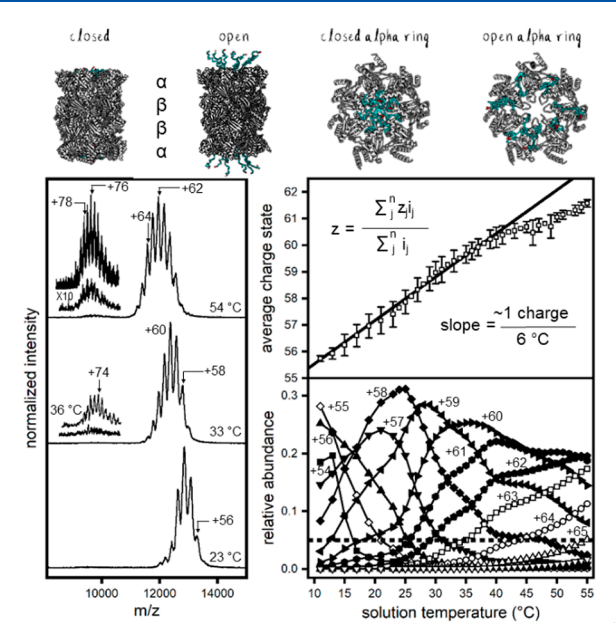


Figure 1. (top) Crystal structure of the 20S proteasome (PDB: 5CZ4). Top, side, and isolated α -ring views show closed and open structures generated by extending α -protein N-termini (blue). (left) Mass spectra for 20S proteasome at 23 °C, 33 °C, and 54 °C. The inset at 54 °C shows examples of high charge state populations (+70 to +79) from two measurements (see SI). (top right) Weighted average charge state as a function of temperature. (bottom right) Relative abundances of +54 to +66 charge states for each temperature. Dotted line indicates 5% abundance level.

(<5%) species, we observe five or six abundant states at nearly every temperature. The transitions between these species are highly coupled. Populating new, higher-charge configurations depletes species accommodating five or six fewer charges. In this way, the 20S charge increases, but the distribution of states remains narrow, suggesting that ensembles of structures and transitions between them are similar. Numerous structural studies indicate that the 20S frame is extremely stable. Structures are dynamic near the N-terminal peptide regions of the α -ring proteins responsible for regulating the proteolytic cavity. We note that five abundant charge states spanning +54 to +59 would require seven additional charges to reach five states spanning +61 to +66. The highly basic amino termini localized in the heptameric α -ring are good candidate sites for proton addition.

In addition to the +54 to +66 particles, above ~ 30 °C, a new population of 20S species (+70 to +79) is observable (Figure 1). These increase in abundance with increasing temperature. However, they comprise only a small percentage of the total ensemble (~ 0.5 to $\sim 2\%$). The +70 to +79 distribution does not overlap in the charge state with the +54 to +66 distribution, indicating a new 20S geometric form.

Additional structural information comes from analyzing IMS cross sections, shown in Figure 2. These data also show that different structures are favored at different temperatures (see SI). Two populations of structures are observed for the +54 to +66 charge states: a compact species ($\Omega \sim 223~\text{nm}^2$), unique to the +54 to +59 charge states, favored from ~11 to 17 °C; and a larger ($\Omega \sim 226~\text{nm}^2$) configuration, favored from ~17 to 33 °C. Formation of the larger conformers is accompanied by depletion of the compact species. Our analysis indicates that these configurational changes are coupled with addition of

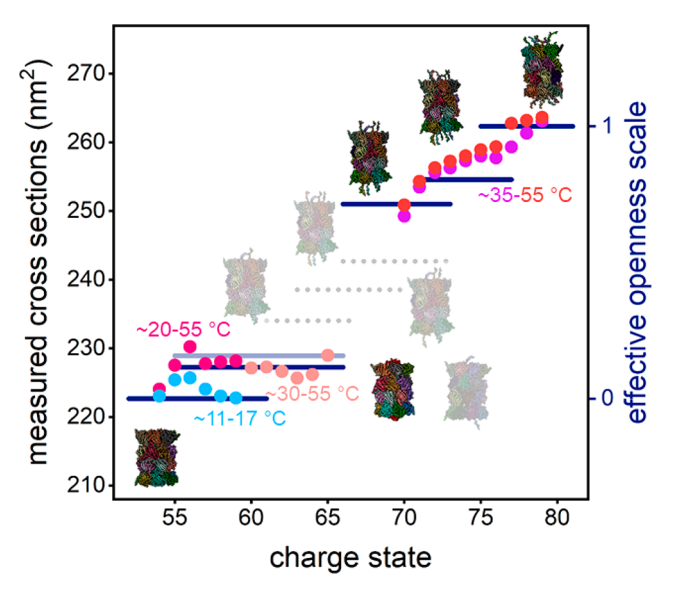


Figure 2. Cross sections plotted as measured (left) and on a normalized effective openness scale (right). Blue and red circles represent +54 to +59 at the indicated temperatures; peach circles represent +60 to +66; and purple and red circles represent +70 to +79 families. Horizontal lines (navy) indicate calculated values of effective openness for candidate structures obtained upon stepwise extension of N-terminal α -ring proteins. Example configurations having calculated values that are not in good agreement with the experiment are indicated as transparent structures. See text and SI for details.

charge (see SI). ¹¹ The low abundance +70 to +79 species are much larger: $\Omega \sim 250-255 \text{ nm}^2$ for +70 to +72, favored from \sim 35 to 45 °C, and $\Omega \sim 260-265 \text{ nm}^2$ for the largest +77 to +79 states. A slight shift to higher cross sections with increasing temperatures is also observed for these configurations.

The experimental finding that 20S cross sections vary over a range of ~18% [i.e., $\Omega(+79) = 264 \text{ nm}^2$ compared with $\Omega(+54) = 223 \text{ nm}^2$ provides a means of bracketing calculated cross sections from crystallographic or other coordinates. Although we cannot rule out the possibility that these cross sections correspond to other regions of the core armature, several observations suggest that multiple axial gate configurations are most consistent with our findings. Numerous highresolution structures show that the stack of four heptameric protein rings that frame the main armature are highly conserved. 12 In contrast, images of the N-terminal regions of the α -ring proteins are poorly defined, indicating that these regions are highly dynamic. 13 These opening ↔ closing transitions are also consistent with the measured reversibility of this system. With this assumption, the calculated range of cross sections for the smallest (closed) and largest (open) configurations is ~16%. This allows us to develop a relative effective openness scale that spans a range of cross sections for anticipated structures (see SI). By definition, an entirely closed-pore particle has an openness of 0.0; an entirely openpore configuration has an openness of 1.0 (Figure 2). The range of experimental values varies by nearly the same factor, allowing us to convert the measured cross section values to this relative scale. From this, we assign the +54 to +66 configurations to a closed form and a second slightly larger closed form that might have N-terminal peptides from the α ring protruding on each side of the core. The +70 to +76 species span a range of open structures. We note that

symmetric structures that are partially open at both ends appear to be most consistent with our analysis (see SI) and in agreement with allosteric transitions observed by others. 14 Our data are inconsistent with each axial gate of the 20S opening independently. The +72 to +76 cross sections are similar to calculated values for open gates, where all but one N-termini are extended. The +77 to +79 states are completely open.

With these assignments, we examine relative stabilities of different structures. Equilibrium populations can be converted into Gibbs free energies using $\Delta G = -RT \ln(K_{eq})$. Figure 3

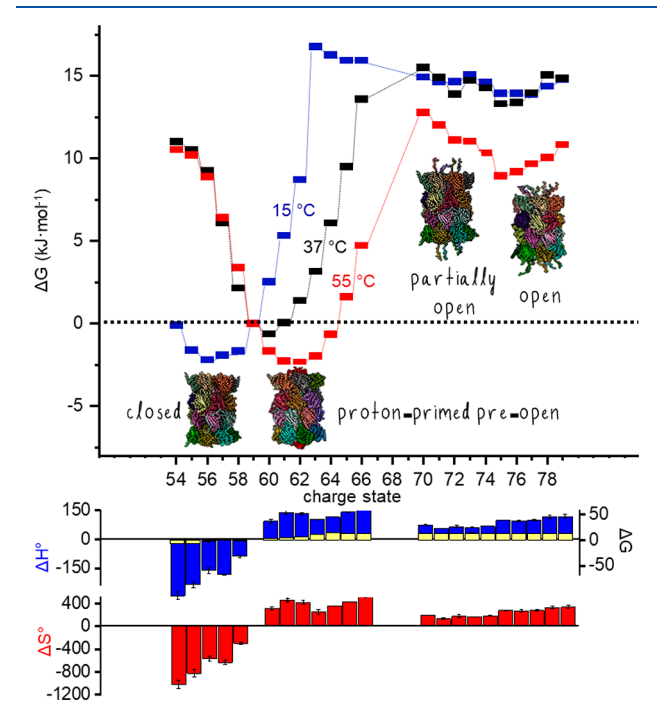


Figure 3. (top) ΔG values for each charge state at three temperatures (15 °C, 37 °C, 55 °C). Values were derived in reference to the +59 state. Structures posited to correspond to observed changes in ΔG are shown. (bottom) Histograms show ΔG (kJ·mol⁻¹, yellow), ΔH° (kJ·mol⁻¹, blue), and ΔS° (J·K⁻¹·mol⁻¹, red) for each charge state at 298 K.

shows free energy landscapes for opening and closing the pore at 15, 37, and 55 °C. Compact, fully closed (+54 to +59) species are favored at 15 °C. At higher temperatures, these structures become unfavorable, and slightly larger (+60 to +66) configurations are favored. Open-pore (+70 to +79) conformers are unfavorable; but of these, the highly open (+74 to +79) configurations are lowest in energy. The scant evidence for partially open forms (having two or three extended N-terminal regions at each end) indicates that it is favorable for N-terminal chains to open together—a cooperative transition.

Derivation of enthalpic and entropic terms provides clues about why different configurations are observed. Figure 3 shows values of ΔH°_{298} and ΔS°_{298} derived from Van 't Hoff analyses for all charge states (see SI). Individual charge state configurations fall into three types of structures. The most compact +54 to +58 closed-pore species are energetically stabilized (average $\Delta H^{\circ}_{298} \sim -192 \text{ kJ} \cdot \text{mol}^{-1}$) but disfavored entropically (average $\Delta S^{\circ}_{298} \sim -668 \text{ J} \cdot \text{K}^{-1} \cdot \text{mol}^{-1}$). Enthalpic favorability arises because of intramolecular binding interactions associated with closing the pore gates. As the closed-

pore configurations tighten, they become less accessible, consistent with a large entropic barrier. In contrast, the +61 to +66 closed-pore configurations are energetically unstable $(\Delta H^{\circ}_{298} \sim 129 \text{ kJ} \cdot \text{mol}^{-1})$ but entropically favored $(\Delta S^{\circ}_{298} \sim$ 400 J·K⁻¹·mol⁻¹). Although the pore remains closed, the addition of charge has loosened the axial gates. It is perhaps not surprising that thermochemistry for the more open (+70 to +79) configurations ($\Delta H^{\circ}_{298} \sim 86 \text{ kJ} \cdot \text{mol}^{-1}$ and $\Delta S^{\circ}_{298} \sim 230$ $J \cdot K^{-1} \cdot mol^{-1}$) is similar to that for the (+60 to +66) configurations. The tightly closed (+54 to +58) configurations have largely disappeared at temperatures where the open-pore (+70 to +79) configurations are observed. From this, we see that the mechanism for opening a closed pore appears to require an entropically favored, charge-primed, preopen state. It is interesting that the open-pore configurations that emerge upon addition of charge to the +60 to +66 forms are enthalpically favorable transitions (i.e., $\Delta H^{\circ}_{298} \sim -300$ kJ· mol^{-1} for (+60 to +66) \rightarrow (+70 to +79)), an indication of the formation of additional structure upon pore opening. Perhaps the protruding N-termini become stiffer, or access to the pore involves many favorable interactions—or both.

ASSOCIATED CONTENT

Supporting Information

The Supporting Information is available free of charge at https://pubs.acs.org/doi/10.1021/acs.jpclett.3c01040.

Experimental methods and detailed description of cross section and thermodynamic analyses (PDF)

AUTHOR INFORMATION

Corresponding Authors

David E. Clemmer – Department of Chemistry, Indiana University, Bloomington, Indiana 47401, United States; orcid.org/0000-0003-4039-1360; Email: clemmer@indiana.edu

Andreas Matouschek — Department of Molecular Biosciences, University of Texas, Austin, Texas 78712, United States; orcid.org/0000-0001-6016-2341; Email: matouschek@austin.utexas.edu

Authors

Lucas W. Henderson — Department of Chemistry, Indiana University, Bloomington, Indiana 47401, United States

Edie M. Sharon — Department of Chemistry, Indiana University, Bloomington, Indiana 47401, United States

Amit K. S. Gautam — Department of Molecular Biosciences, University of Texas, Austin, Texas 78712, United States

Adam J. Anthony — Department of Chemistry, Indiana University, Bloomington, Indiana 47401, United States

Martin F. Jarrold — Department of Chemistry, Indiana University, Bloomington, Indiana 47401, United States;

orcid.org/0000-0001-7084-176X

David H. Russell — Department of Chemistry, Texas A&M

David H. Russell — Department of Chemistry, Texas A&M University, College Station, Texas 77843, United States; orcid.org/0000-0003-0830-3914

Complete contact information is available at: https://pubs.acs.org/10.1021/acs.jpclett.3c01040

Author Contributions

(LWH and EMS) These authors contributed equally to this work. LWH and EMS performed experiments and processed data. AKSG generated proteasome samples. AJA processed

proteasome samples prior to experiments. The manuscript was written by DEC, LWH, and EMS. DHR, AM, and MFJ provided insight about modeling and treatment of the data. All authors have given approval to the final version of the manuscript.

Notes

The authors declare the following competing financial interest(s): DEC and MFJ are consultants for the Waters Corp. and co-founders of Megadalton Solutions, a startup company devel-oping charge detection mass spectrometry for analysis of high-mass ions. All of the other authors declare no competing financial conflicts of interest.

ACKNOWLEDGMENTS

This work is supported in part by grants from the National Institutes of Health R01 GM131100, 5R01 GM135246-03, R56DK129592, The Welch Foundation (F-1817), and the National Science Foundation CHE-1904749.

ABBREVIATIONS

IMS, ion mobility spectrometry; MS, mass spectrometry

REFERENCES

- (1) Tanaka, K. The Proteasome: Overview of Structure and Functions. *Proceedings of the Japan Academy, Series B* **2009**, 85 (1), 12–36.
- (2) Davis, C.; Spaller, B. L.; Matouschek, A. Mechanisms of Substrate Recognition by the 26s Proteasome. *Curr. Opin. Struct. Biol.* **2021**, *67*, 161–169.
- (3) Martinez-Fonts, K.; Davis, C.; Tomita, T.; Elsasser, S.; Nager, A. R.; Shi, Y.; Finley, D.; Matouschek, A. The Proteasome 19s Cap and Its Ubiquitin Receptors Provide a Versatile Recognition Platform for Substrates. *Nat. commun* **2020**, *11* (1), 477. Schweitzer, A.; Aufderheide, A.; Rudack, T.; Beck, F.; Pfeifer, G.; Plitzko, J. M.; Sakata, E.; Schulten, K.; Förster, F.; Baumeister, W. Structure of the Human 26s Proteasome at a Resolution of 3.9 Å. *Proc. Natl. Acad. Sci. U. S. A.* **2016**, *113* (28), 7816–7821.
- (4) Sahu, I.; Mali, S. M.; Sulkshane, P.; Xu, C.; Rozenberg, A.; Morag, R.; Sahoo, M. P.; Singh, S. K.; Ding, Z.; Wang, Y.; et al. The 20s as a Stand-Alone Proteasome in Cells Can Degrade the Ubiquitin Tag. *Nat. commun* **2021**, *12* (1), 6173. Kumar Deshmukh, F.; Yaffe, D.; Olshina, M. A.; Ben-Nissan, G.; Sharon, M. The Contribution of the 20s Proteasome to Proteostasis. *Biomolecules* **2019**, *9* (5), 190.
- (5) El-Baba, T. J.; Woodall, D. W.; Raab, S. A.; Fuller, D. R.; Laganowsky, A.; Russell, D. H.; Clemmer, D. E. Melting Proteins: Evidence for Multiple Stable Structures Upon Thermal Denaturation of Native Ubiquitin from Ion Mobility Spectrometry-Mass Spectrometry Measurements. J. Am. Chem. Soc. 2017, 139 (18), 6306–6309.
- (6) Silveira, J. A.; Fort, K. L.; Kim, D.; Servage, K. A.; Pierson, N. A.; Clemmer, D. E.; Russell, D. H. From Solution to the Gas Phase: Stepwise Dehydration and Kinetic Trapping of Substance P Reveals the Origin of Peptide Conformations. *J. Am. Chem. Soc.* 2013, 135 (51), 19147–19153. Raab, S. A.; El-Baba, T. J.; Laganowsky, A.; Russell, D. H.; Valentine, S. J.; Clemmer, D. E. Protons Are Fast and Smart; Proteins Are Slow and Dumb: On the Relationship of Electrospray Ionization Charge States and Conformations. *J. Am. Soc. Mass. Spectrom.* 2021, 32 (7), 1553–1561.
- (7) Daggett, V.; Fersht, A. The Present View of the Mechanism of Protein Folding. *Nat. Rev. Mol. Cell Biol.* **2003**, *4* (6), 497–502. Benesch, J. L.; Sobott, F.; Robinson, C. V. Thermal Dissociation of Multimeric Protein Complexes by Using Nanoelectrospray Mass Spectrometry. *Anal. Chem.* **2003**, *75* (10), 2208–2214. Wang, G.; Bondarenko, P. V.; Kaltashov, I. A. Multi-Step Conformational Transitions in Heat-Treated Protein Therapeutics Can Be Monitored in Real Time with Temperature-Controlled Electrospray Ionization Mass Spectrometry. *Analyst* **2018**, *143* (3), 670–677.

- (8) Vimer, S.; Ben-Nissan, G.; Morgenstern, D.; Kumar-Deshmukh, F.; Polkinghorn, C.; Quintyn, R. S.; Vasil'ev, Y. V.; Beckman, J. S.; Elad, N.; Wysocki, V. H.; et al. Comparative Structural Analysis of 20s Proteasome Ortholog Protein Complexes by Native Mass Spectrometry. ACS Central Science 2020, 6 (4), 573–588. Ben-Nissan, G.; Sharon, M. Regulating the 20s Proteasome Ubiquitin-Independent Degradation Pathway. Biomolecules 2014, 4 (3), 862–884.
- (9) Sahu, I.; Glickman, M. H. Structural Insights into Substrate Recognition and Processing by the 20s Proteasome. *Biomolecules* **2021**, *11* (2), 148.
- (10) Dupuis, N. F.; Wu, C.; Shea, J.-E.; Bowers, M. T. Human Islet Amyloid Polypeptide Monomers Form Ordered B-Hairpins: A Possible Direct Amyloidogenic Precursor. J. Am. Chem. Soc. 2009, 131 (51), 18283–18292. Clemmer, D. E.; Jarrold, M. F. Ion Mobility Measurements and Their Applications to Clusters and Biomolecules. J. Mass Spectrom. 1997, 32 (6), 577–592. McCabe, J. W.; Mallis, C. S.; Kocurek, K. I.; Poltash, M. L.; Shirzadeh, M.; Hebert, M. J.; Fan, L.; Walker, T. E.; Zheng, X.; Jiang, T.; et al. First-Principles Collision Cross Section Measurements of Large Proteins and Protein Complexes. Anal. Chem. 2020, 92 (16), 11155–11163. Ruotolo, B. T.; Benesch, J. L.; Sandercock, A. M.; Hyung, S.-J.; Robinson, C. V. Ion Mobility—Mass Spectrometry Analysis of Large Protein Complexes. Nat. Protoc. 2008, 3 (7), 1139–1152.
- (11) Shi, L.; Holliday, A. E.; Khanal, N.; Russell, D. H.; Clemmer, D. E. Configurationally-Coupled Protonation of Polyproline-7. *J. Am. Chem. Soc.* **2015**, *137* (27), 8680–8683.
- (12) Reinheckel, T.; Sitte, N.; Ullrich, O.; Kuckelkorn, U.; Davies, K. J.; Grune, T. Comparative Resistance of the 20s and 26s Proteasome to Oxidative Stress. *Biochem. J.* **1998**, 335 (3), 637–642.
- (13) Groll, M.; Bajorek, M.; Köhler, A.; Moroder, L.; Rubin, D. M.; Huber, R.; Glickman, M. H.; Finley, D. A Gated Channel into the Proteasome Core Particle. *Nat. Struct. Biol.* 2000, 7 (11), 1062–1067. (14) Yu, Z.; Yu, Y.; Wang, F.; Myasnikov, A. G.; Coffino, P.; Cheng, Y.; et al. Allosteric Coupling between A-Rings of the 20s Proteasome. *Nat. commun* 2020, 11 (1), 4580.
- (15) El-Baba, T. J.; Clemmer, D. E. Solution Thermochemistry of Concanavalin a Tetramer Conformers Measured by Variable-Temperature Esi-Ims-Ms. *Int. J. Mass spectrom.* **2019**, *443*, 93–100. Raab, S. A.; El-Baba, T. J.; Woodall, D. W.; Liu, W.; Liu, Y.; Baird, Z.; Hales, D. A.; Laganowsky, A.; Russell, D. H.; Clemmer, D. E. Evidence for Many Unique Solution Structures for Chymotrypsin Inhibitor 2: A Thermodynamic Perspective Derived from Vt-Esi-Ims-Ms Measurements. *J. Am. Chem. Soc.* **2020**, *142* (41), 17372–17383.